LA-UR-07-6854

Title: The Moment-of-Fluid Method in Action

Author(s):
Hyung Taek Ahn (T-7, htahn@lanl.gov)
Mikhail Shashkov (T-7, shashkov@lanl.gov)
Mark A. Christon (CCS-2, christon@lanl.gov)

Intended for:
To be presented at
Third Asian-Pacific Congress on Computational Mechanics
(APCOM'07), Dec. 3-6, 2007, Kyoto, Japan

The Moment-of-Fluid Method in Action

Hyung Taek Ahn*,[1], Mikhail Shashkov[2], Mark A. Christon[3]
[1,2] T-7, Los Alamos National Laboratory, Los Alamos, NM 87545, USA
[3] CCS-2, Los Alamos National Laboratory, Los Alamos, NM 87545, USA
e-mails: htahn@lanl.gov, shashkov@lanl.gov, christon@lanl.gov

Abstract

The Moment-of-Fluid (MOF) method is a new volume-tracking method that accurately treats evolving material interfaces. The MOF method uses moment data, namely the material volume fraction, as well as the centroid, for a more accurate representation of the material configuration, interfaces and concomitant volume advection. In contrast, the Volume-of-Fluid (VOF) method uses only volume fraction data for interface reconstruction and advection. Based on the moment data for each material, the material interfaces are reconstructed with second-order spatial accuracy in a strictly conservative manner. The MOF method is coupled with a stabilized finite element incompressible Navier-Stokes solver for two materials. The effectiveness of the MOF method is demonstrated with a free-surface dam-break and a two-material Rayleigh-Taylor problem.

Key words: moment-of-fluid (MOF), volume-of-fluid (VOF), interface reconstruction, multiphase flow, stabilized finite element

1 Introduction

The moment-of-fluid method [4, 2] can be thought of as a generalization of the volume-of-fluid method. In the VOF method, volume (the zeroth moment) is advected with a local velocity and the interface is reconstructed based on updated volume fraction data. In the MOF method, both volume and the material centroid data (ratio of the first moment with respect to the zeroth moment) are advected and the interface is reconstructed based on the updated moment data, material volume and centroid.

By using the centroid information, volume-tracking with dynamic interfaces can be performed much more accurately. Furthermore, using the moment data permits the interface in a given computational cell to be reconstructed independently from its neighbor cells – a significant computational advantage. With the advantages of the MOF method over the VOF method, our opinion is that the MOF method is the next generation of volume-tracking for interfacial flow computations.

This paper is organized as follows. In §2 we review the piecewise linear interface calculation (PLIC) methods and the standard MOF interface reconstruction method. In §3, a brief

overview of the stabilized finite element formulation and solution procedure is presented. Results from the broken-dam and Rayleigh-Taylor simulations are discussed in §4. Finally, we summarize our findings and conclusions for this work.

2 Moment-of-fluid method

This section begins with a brief review of the piecewise linear interface calculation (PLIC) method and the computation of truncated volumes in the VOF method. The primary concepts for the MOF reconstruction procedure are outlined, and the concomitant moment advection algorithm is described.

2.1 Piecewise linear interface calculation

Most modern VOF methods rely on a PLIC procedure for locating material interfaces and computing the truncated material volume in a computational cell. Using PLIC, each interface between two materials in a mixed cell is represented by a line (plane in 3D). It is convenient to specify this line in *Hessian normal form*,

$$\mathbf{n} \cdot \mathbf{r} + d = 0\,, \tag{1}$$

where $\mathbf{r} = (x, y)$ is a point on the interface, $\mathbf{n} = (n_x, n_y)$ are components of the unit normal to the interface, and d is the signed distance from the origin to the interface.

The principal constraint for locating the planar interface in a cell is local volume conservation, i.e., the reconstructed interface must truncate a cell, c, with a volume equal to the volume of the material V_c^{ref} in the cell. The volume fraction is defined as $f_c^{ref} = V_c^{ref}/V_c$, where V_c is the volume of the entire cell c.

PLIC methods differ primarily in how the interface normal $\mathbf{n}$ is computed. In Youngs' VOF method [10, 11], the interface normal ($\mathbf{n}_i$) for cell-i is computed from the volume fraction data on the stencil composed of cell-i and its immediate neighbors. In the MOF method, the interface normal ($\mathbf{n}_i$) for cell-i is computed from moment data, i.e., volume fraction and material centroids, on cell-i only. Once the interface normal $\mathbf{n}$ is computed, the interface is uniquely defined by computing d so that the truncated material volume V_c^{ref} is matched exactly. In flux-based advection schemes, the interface location is used to partition the advection flux volume by material, and may lead to numerical errors for face-based advection schemes.

2.2 Moment-of-fluid interface reconstruction

The *moment-of-fluid* interface reconstruction method was first introduced by Dyadechko and Shashkov [4] for interface reconstruction in 2D. The MOF method uses the volume fraction, f_c^{ref}, and the material centroid, $\mathbf{x}_c^{ref}$, but *only* for each cell c under consideration. No information from neighboring cells is used, as illustrated in Fig. 1.

The computed interface is chosen to match the reference volume exactly and to provide the best possible approximation to the reference centroid of the material. That is, in MOF,

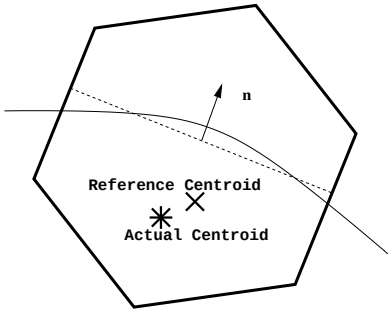

Figure 1: Stencil for the MOF error computation in two dimensions. The stencil is composed of only the cell under consideration. The solid curved line represents the true interface, and the dashed straight line represents the piecewise linear, volume fraction matching interface at the cell. The method is transparent to the topology of the cell shape, i.e. polygonal cells (polyhedral cells in 3D) can be utilized without extra complexity.

the interface normal, $\mathbf{n}$, is computed by minimizing the functional,

$$E_c^{MOF}(\mathbf{n}) = \| \mathbf{x}_c^{ref} - \mathbf{x}_c(\mathbf{n}) \|^2 \tag{2}$$

under the constraint that the volume fraction for the truncated cell exactly matches the reference volume fraction. Here, $\mathbf{x}_c^{ref}$ is the reference material centroid and $\mathbf{x}_c(\mathbf{n})$ is the actual (reconstructed) material centroid with given interface normal $\mathbf{n}$.

The minimization of the non-linear functional, $E_c^{MOF}(\mathbf{n})$, requires three steps. The first step is to find the parameter d for a plane such that the volume fraction in cell c exactly matches f_c^{ref}. Second, the centroid of the resulting truncated cell is computed. This is a simple calculation and is described in [1]. Finally, the distance between the actual and reference centroids is computed. The MOF method reconstructs linear interfaces exactly, i.e., it is "linearity-preserving".

2.3 Moment advection scheme

In order to apply the MOF reconstruction to volume-track evolving interfaces, a moment advection scheme is required. Similar to VOF, various types of advection schemes can be devised for MOF. For example, a flux-based approach or a Lagrange+remap approach can be used. The advection scheme presented here is based on remapping from a Lagrangian pre-image based on a characteristic backtrace.

The moment advection is performed only for the *potentially-mixed* cells, i.e., the cells that may contain a material interface. The potentially-mixed cells are determined by checking the following two conditions:

1. if cell-c or any of its neighbors is mixed, i.e., contains more than one material,

2. if cell-c is a pure cell, and any of its neighbors is a pure cell but with a different material.

These two conditions are devised to detect when material interface exist inside of the local neighbor stencil of cell-c. We note that more potentially-mixed cells can be identified by

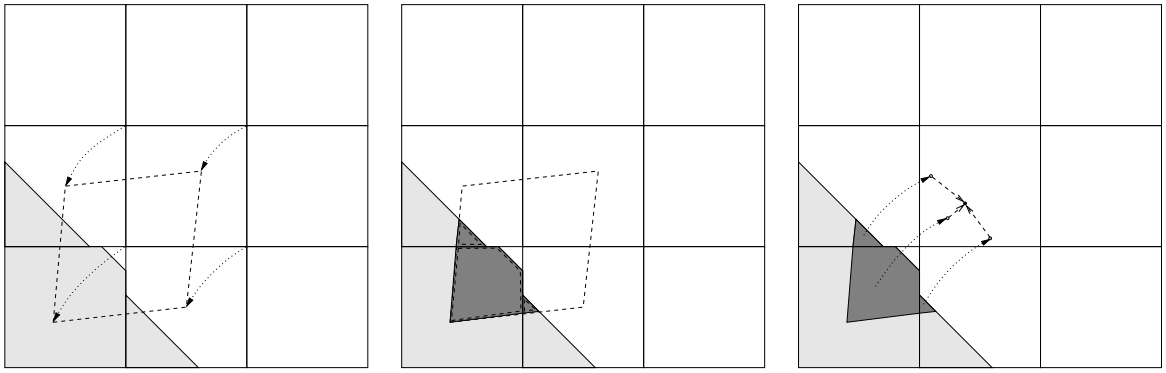

(a) Lagrangian backtrace (b) polygon intersection (c) centroid advection

Figure 2: Moment advection by Lagrange+remap strategy. The moment advection process for the central cell-c on 3×3 local stencil is illustrated.

using a wider stencil – a necessary consideration for $CFL > 1$ calculations. For all test cases presented in this paper, the time steps are chosen in accordance with $CFL \leq 1$. Hence, the local stencil is composed of only the immediate neighbors and the number of potentially-mixed cells that reside within a narrow band around the interface.

The present advection method is composed of the follows steps:

1. Lagrangian backtrace
2. polygon intersection (reference volume computation)
3. centroid advection (reference centroid computation)

The three conceptual stages of the advection scheme are illustrated in Fig. 2. First, in the Lagrangian-backtrace step, a cell-c is traced backward in time along characteristics using the local velocity. In Fig. 2-(a), the backtrace of the central cell-c in a 3×3 mesh is illustrated. With the cell configuration associated with the Lagrangian backtrace, the material regions, to be remapped on the backtraced cell, can be computed by a direct polygon-polygon intersection. Once the intersection is carried out, a set of polygons representing the material to be remapped to cell-c are defined. These intersected polygons, indicated by dark gray in Fig. 2-(b), contain the amount of volume to be occupied by the cell-c at the next time step. The amount of volume advected to cell-c can be computed as

$$\mathcal{V}^{ref} = \sum_{p \in \mathcal{P}_{backward}} \mathcal{V}_p \tag{3}$$

where $\mathcal{P}_{backward}$ indicates the set of polygons obtained by intersection of backtraced cell and material subcells in the local stencil and $\mathcal{V}_p$ is the volume of polygon-p.

The reference volume $\mathcal{V}^{ref}$ to be remapped on cell-c may be *incompatible* with cell-c in two ways. First, $\mathcal{V}^{ref}$ may not fit in cell-c, i.e., $\mathcal{V}^{ref} > \mathcal{V}_c$. In this situation, cell-c is *overfilled*. If a cell is overfilled, then the excess volume $\Delta\mathcal{V}_{over} = \mathcal{V}^{ref} - \mathcal{V}_c$ is distributed to the *mixed* neighbor cells. Typically this can be done with a sweep over the immediate cell neighbors. If the cell is still overfilled, that is the mixed neighbors cannot accommodate

more material without becoming overfilled, then the overfilled repair sweep extends to the next set of immediate neighbors, and so on.

The second volume advection incompatibility is the *underfilled* case. If the Lagrangian pre-image for cell-c in Fig. 2 contains only the primary material (e.g., only the gray material and no white material), and the reference volume $\mathcal{V}^{ref}$ is not sufficient to fill cell-c completely, i.e., $\mathcal{V}^{ref} < \mathcal{V}_c$, then cell-$c$ is underfilled. If a cell is underfilled, then the underfilled amount $\Delta\mathcal{V}_{under} = \mathcal{V}_c - \mathcal{V}^{ref}$ can be borrowed from its *mixed* neighbors. Again, this type of volume repair is done with a sweep through immediate cell neighbors. If the cell is still underfilled, that is the mixed neighbors cannot donate more volume, the repair sweep extends to the next set of immediate neighbors, and so on. We note that the overfilled and underfilled cases are typically equally-balanced within the local neighbor stencil around a given cell [7]. For the computations presented below, we first perform the overfilled repair, and then the underfilled repair step.

Finally, for the centroid update, the centroids of the polygons contained in the set $\mathcal{P}_{backward}$ are traced forward in time using the local velocity, as shown in Fig. 2-(c). The reference centroid for the advected volume is computed by the volume weighted sum of forward traced centroids, and expressed as follows

$$\mathbf{x}_c^{ref} = \frac{\sum_{p\in\mathcal{P}_{backward}} \mathbf{x}_p^{forward}\mathcal{V}_p}{\sum_{p\in\mathcal{P}_{backward}} \mathcal{V}_p} \tag{4}$$

where $\mathbf{x}_p^{forward}$ represents the forward traced centroid associated with polygon p.

The backward and forward traces both require a velocity field that can be evaluated at arbitrary locations in space and time. For a prescribed analytical velocity field that is defined as a function of position and time, $\mathbf{v} = \mathbf{v}(\mathbf{x}, t)$, the local velocity can be easily evaluated at a given position $\mathbf{x}$ and time t. When MOF is coupled with a flow solver, the required velocities can be obtained by interpolating the velocities computed by the flow solver. In this work, we exploit the node-centered velocities used in the stabilized finite element solver.

3 Flow solution algorithm

In this section, we present the variable-density incompressible Navier-Stokes equations, and the stabilized finite element formulation. A brief overview of the solution procedure that couples the stabilized finite element solver with the MOF volume-tracking method is discussed.

3.1 Incompressible Navier-Stokes equations

Let $\mathbf{\Omega}$ be the spatial domain, and let Γ be the boundary of Ω. We consider the following velocity-pressure formulation of the incompressible Navier-Stokes equation for two immiscible fluids.

$$\rho\left(\frac{\partial \mathbf{u}}{\partial t} + \mathbf{u}\cdot\nabla\mathbf{u} - \mathbf{f}\right) - \nabla\cdot\sigma = \mathbf{0} \quad in \quad \Omega\times[0,T] \tag{5}$$

$$\nabla \cdot \mathbf{u} = 0 \quad in \quad \Omega \times [0, T] \tag{6}$$

where $\rho = f^1\rho^1 + f^2\rho^2$ is the mixture density, $\mathbf{u}$ is the velocity, $\mathbf{f}$ is the body force, and σ is the stress tensor defined by

$$\sigma(p, \mathbf{u}) = -p\mathbf{I} + 2\mu\epsilon(\mathbf{u}), \tag{7}$$

with

$$\epsilon(\mathbf{u}) = \frac{1}{2}\left(\nabla\mathbf{u} + (\nabla\mathbf{u})^T\right). \tag{8}$$

Here p is the pressure, $\mu = f^1\mu^1 + f^2\mu^2$ is the mixture dynamic viscosity, and $\mathbf{I}$ is the identity tensor.

The Dirichlet and Neumann boundary conditions prescribed on Γ can be represented by

$$\mathbf{u} = \mathbf{g} \quad on \quad \Gamma_g, \tag{9}$$

$$\mathbf{n} \cdot \sigma = \mathbf{h} \quad on \quad \Gamma_h, \tag{10}$$

where Γ_g and Γ_h are complementary subsets of Γ.

3.2 Stabilized finite element formulation

The stabilized finite formulation follows the method outlined in [9]. We begin with suitably defined finite-dimensional trial and test function spaces for velocity and pressure, $\mathcal{S}^h_{\mathbf{u}}$, $\mathcal{V}^h_{\mathbf{u}}$, $\mathcal{S}^h_p$, and $\mathcal{V}^h_p = \mathcal{S}^h_p$.

The finite element problem can be expressed as follows. Find $\mathbf{u}^h \in \mathcal{S}^h_{\mathbf{u}}$ and $p^h \in \mathcal{S}^h_p$ such that $\forall \mathbf{w}^h \in \mathcal{V}^h_{\mathbf{u}}$ and $\forall q^h \in \mathcal{V}^h_p$

$$\begin{aligned}\int_\Omega \mathbf{w}^h \cdot \left(\frac{\partial \mathbf{u}^h}{\partial t} + \mathbf{u}^h \cdot \nabla\mathbf{u}^h - \mathbf{f}\right) d\Omega + \int_\Omega \epsilon(\mathbf{w}^h) : \sigma^h d\Omega - \int_\Gamma \mathbf{w}^h \cdot \mathbf{h} d\Gamma + \int_\Gamma q^h \nabla \cdot \mathbf{u}^h d\Omega \\ + \sum_{e=1}^{n_{el}} \int_{\Omega^e} \frac{1}{\rho}\left[\tau_{SUPG}\rho\mathbf{u}^h \cdot \nabla\mathbf{w}^h + \tau_{PSPG}\nabla q^h\right] \cdot \left[\rho\left(\frac{\partial \mathbf{u}^h}{\partial t} + \mathbf{u}^h \cdot \nabla\mathbf{u}^h\right) - \nabla \cdot \sigma - \rho\mathbf{f}\right] d\Omega^e \\ + \sum_{e=1}^{n_{el}} \int_{\Omega^e} \tau_{LSIC}\nabla \cdot \mathbf{w}^h \rho \nabla \cdot \mathbf{u}^h d\Omega^e = 0.\end{aligned} \tag{11}$$

In the above equation, the first line originated from the Galerkin formulation of the incompressible Navier-Stokes equations, and the following two terms from the stabilization introduced on each element interior. Note that the stabilization terms are evaluated as the sum of element integrals where n_{el} is the number of elements in the discretized computational domain. The first two stabilization terms, associated with τ_{SUPG} and τ_{PSPG}, correspond to streamline-upwind/Petrov-Galerkin (SUPG) [3] and pressure-stabilizing/Petrov-Galerkin (PSPG) [8] respectively. The last stabilization term, indicated by τ_{LSIC}, is the least-squares stabilization on the incompressibility constraint (LSIC) [9], which is essentially an additional dissipation for high Reynolds number flows.

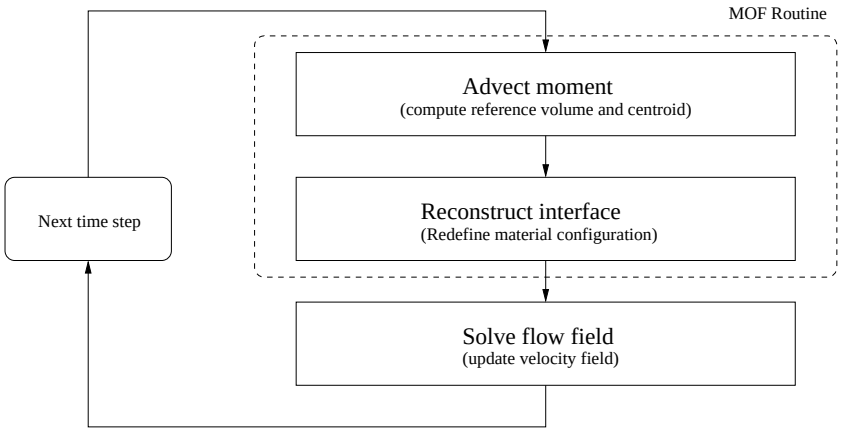

Figure 3: Solution procedure for volume-tracking interfacial flow with the moment-of-fluid (MOF) method.

For our work, we adopt the stabilization parameters defined by Tezduyar et al. [8, 9].

$$\tau_{SUPG} = \tau_{PSPG} = \left[\left(\frac{2||\mathbf{u}^h||}{h} \right)^2 + 9 \left(\frac{4\nu}{h^2} \right)^2 \right]^{-1/2} \tag{12}$$

and

$$\tau_{LSIC} = \frac{||\mathbf{u}^h||h}{2} \tag{13}$$

Here $\mathbf{u}^h$ is the local velocity vector, h is the local length scale, and ν is the kinematic mixture viscosity.

The discretization of Eq. (11) results in a nonlinear system of equations to be solved at each time step. The implementation of our solver is based on LibMesh [5], a C++ finite element library.

3.3 Coupling with MOF volume-tracking method

The solution procedure for the coupled stabilized finite element – MOF methods is shown in Fig. 3. The two solution modules are loosly coupled, with independent time-integrators for each modules, i.e. explicit forward-Euler for the MOF advection and implicit backward-Euler for the flow solver.

4 Results

The efficacy of the MOF method for volume-tracking interfacial flows is demonstrated with two example problems, namely the broken-dam and Rayleigh-Taylor problems.

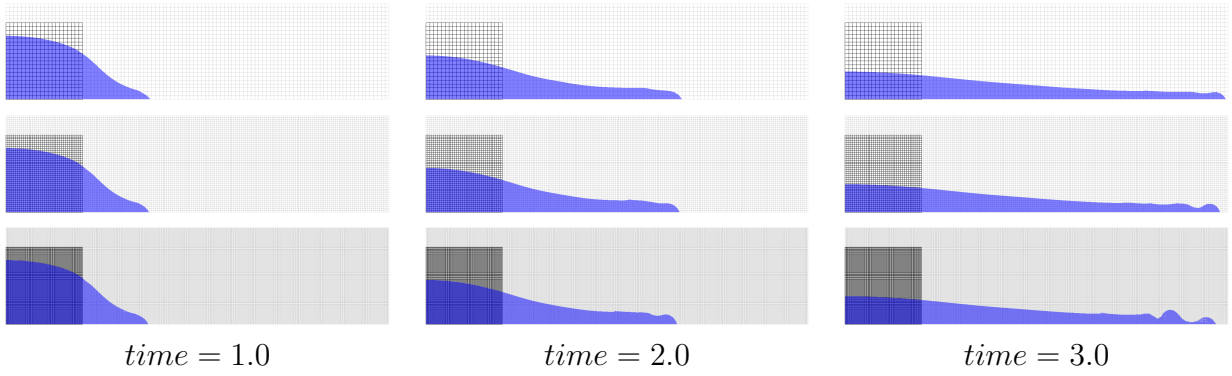

Figure 4: Snapshots of the water-air interface for the dam-break problem. Three different meshes, coarse (top, 100x25), medium (middle, 200x50), and fine (bottom, 400x100) are used. Snapshots are taken at three different non-dimensional time steps. The instantaneous water configuration is indicated by the blue (transparent) regions, and the initial configuration of the water column is indicated by the dark mesh lines.

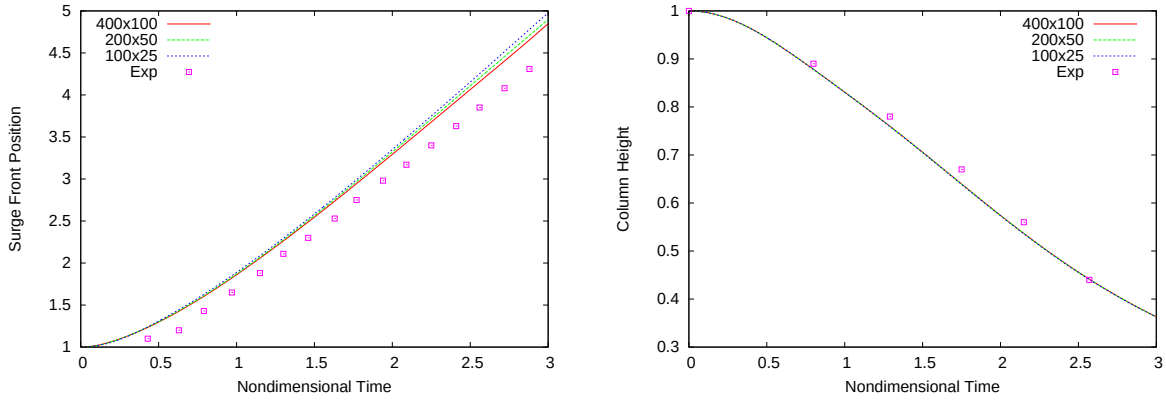

Figure 5: Surge front position and column height comparison with experimental data [6].

4.1 Dam-Break

The collapse of a water column under gravitational acceleration is known as the dam-break problem. A computational domain of $[0, 5a] \times [0, 1.25a]$ is considered where $a = 0.05715m$ is the height of water column in its initial configuration. The Reynolds number based on the length scale is $Re = 42792$, and the density and viscosity ratios are $\rho_{water}/\rho_{air} = 1/.001$ and $\mu_{water}/\mu_{air} = 1/.01$. The nondimensional time scale is given by $t\sqrt{g/a}$ where $g = 9.81m/s^2$ is the gravitational acceleration. Results from the MOF/stabilized finite element calculations are shown in Fig. 4, and also compared with experimental results [6] in Fig. 5.

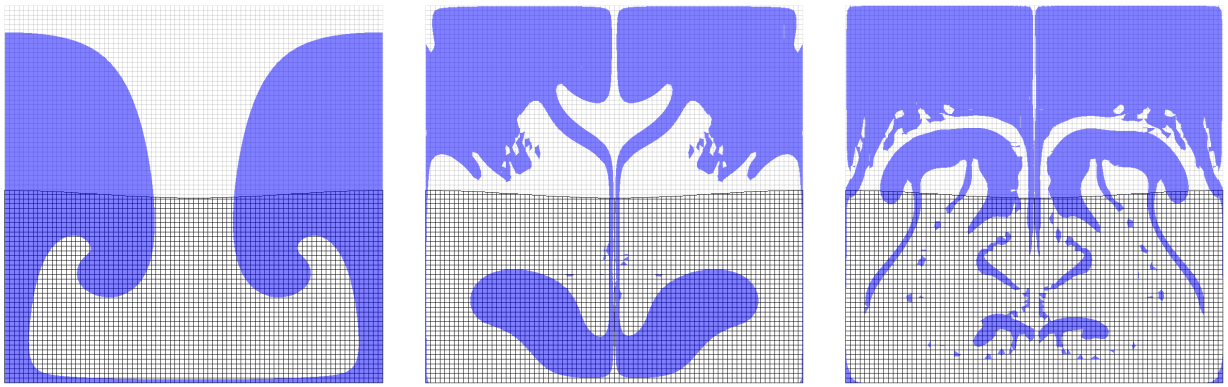

$time = 0.5$ $time = 1.0$ $time = 1.5$

Figure 6: Snapshots, taken at different nondimensional timesteps, of the Rayleigh-Taylor instability problem. 80^2 mesh is used. The initial configuration of the light material is indicated by dark mesh lines and its instantaneous configuration is indicated by blue (transparent) regions.

4.2 Rayleigh-Taylor Instability

The Rayleigh-Taylor instability occurs when a heavy fluid is accelerated by a light fluid. For the test problem, the domain of $[0, 1]^2$ discretized with 80^2 mesh is considered. The heavy fluid occupies the top half of the domain and the light fluid is located on the bottom half of the domain. The initial interface is perturbed to accelerate the mixing. The density and viscosity ratios are $\rho_{heavy}/\rho_{light} = 1/.5$ and $\mu_{heavy}/\mu_{light} = 1/.5$. The Reynolds number is chosen as $Re = 283$. The computational results are shown in Fig. 6. It is clear that small size bubbles and thin filaments within the tolerance of local mesh size are correctly resolved in the present results.

5 Conclusions

The moment-of-fluid method, a new volume-tracking method, has been successfully applied to two-fluid incompressible interfacial flow simulations. Two representative test cases were demonstrated, namely broken-dam and Rayleigh-Taylor instability problem. The current computational results are compared with available experimental data and show good agreement. It is also observed that the small scale feature, such as bubbles and filaments, can be well resolved with the present MOF method. Futher comparative studies with more traditional VOF type methods are to be presented in our forthcoming reports.

Acknowledgments. This work was carried out under the auspices of the National Nuclear Security Administration of the U.S. Department of Energy at Los Alamos National Laboratory under Contract No. DE-AC52-06NA25396 and the DOE Office of Science Advanced Scientific Computing Research (ASCR) Program in Applied Mathematics Research. This work was supported by the Advanced Simulation and Computing (ASC) program at the Los Alamos National Laboratory.

References

[1] H. T. Ahn and M. Shashkov. Geometric algorithms for 3d interface reconstruction. In *16th International Meshing Roundtable*, 2007.

[2] H. T. Ahn and M. Shsahkov. Multi-material interface reconstruction on generalized polyhedral meshes. *Journal of Computational Physics*, 226:2096–2132, 2007.

[3] A.N. Brooks and T.J.R. Hughes. Streamline-upwind/petrov-galerkin formulations for convection dominated flows with particular emphasis on the incompressible navier-stokes equation. *Computer Methods in Applied Mechanics and Engineering*, 32:199–259, 1982.

[4] V. Dyadechko and M. Shashkov. Moment-of-fluid interface reconstruction. Technical Report LA-UR-05-7571, Los Alamos National Laboratory.

[5] B. S. Kirk, J. W. Peterson, R. Stogner, and S. Petersen. Libmesh: A C++ finite element library, 2006. http://libmesh.sourceforge.net/.

[6] J.C. Martin and W.J. Moyce. An experimental study of the collapse of liquid columns on a rigid horizontal plane. *Philosophical Transactions of the Royal Society of London, Series A. Mathematical, Physical and Engineering Sciences*, 244:312–324, 1952.

[7] M. Shashkov and B. Wendroff. The repair paradigm and application to conservation laws. *Journal of Computational Physics*, 198:265–277, 2004.

[8] T.E. Tezduyar, S. Mittal, S.E. Ray, and R. Shih. Incompressible flow computations with stabilized bilinear and linear equal-order-interpolation velocity-pressure elements. *Computer Methods in Applied Mechanics and Engineering*, 95:221–242, 1992.

[9] T.E. Tezduyar and Y. Osawa. Finite element stabilization parameters computed from element matrices and vectors. *Computer Methods in Applied Mechanics and Engineering*, 190:411–430, 2000.

[10] D. L. Youngs. *Numerical Methods for Fluid Dynamics*, chapter Time-Dependent Multi-material flow with large fluid distortion, pages 273–285. Academic Press, 1982.

[11] D. L. Youngs. An interface tracking method for a 3D Eulerian hydrodynamics code. Technical Report AWRE/44/92/35, Atomic Weapons Research Establishment, Design Mathematics Division, Aldermaston, Reading, Berkshire, United Kingdom, 1987.